Sensors & Actuators: B. Chemical 281 (2019) 1080–1087

Contents lists available at ScienceDirect

Sensors and Actuators B: Chemical

journal homepage: www.elsevier.com/locate/snb

Carbon nanotube thin-film-transistors for gas identification

Jialuo Chen[a,*], Ardalan Lotfi[b], Peter J. Hesketh[b], Satish Kumar[b]

[a] School of Electrical and Computer Engineering, Georgia Institute of Technology, Atlanta 30332, USA
[b] G. W. Woodruff School of Mechanical Engineering, Georgia Institute of Technology, Atlanta 30332, USA

ARTICLE INFO

Keywords:
CNT-TFTs
Gas sensors
Low ppm concentration
Gas identification
Sensing mechanism

ABSTRACT

Single-walled carbon nanotube (CNT) based gas sensors have enormous potential in pollution monitoring in low concentration level because of its high sensitivity, fast response, and physical/chemical stability. However, the lack of selectivity has been a major drawback for its wide range employment. In this work, we fabricate thin film transistors (TFTs) using randomly distributed CNTs and investigate them for ammonia and nitrogen dioxide detection in air at low ppm concentrations. A sensing mechanism is proposed based on the interaction between gas molecules and different types of dwelling spots inside the channel area of a TFT. We present double exponential-convolution model to decipher sensor response as well as to explore its application in gas identification. In this context, the consistency in time constants is recognized, which is independent of gas concentration. More importantly, the time constants vary with respect to different gas types and TFTs. The uniqueness of time constants can work as identity verification for different sensing gases, which demonstrates that the sensor response is a distinctive behavior determined by the unique channel structure of each TFT. This work provides us a general strategy for gas identification in ppm level and a practical path to realize the advantages of CNT gas sensors in air quality detection as well as the industrial emission control.

1. Introduction

Single-walled carbon nanotube (SWCNT) based sensors have been widely studied due to their significant advantages in monitoring different gases at low ppm/ppb level [1–6]. As a new generation of semiconducting material, SWCNT based devices have very low power consumption [7], fast operation speed [8], and high flexibility [9–11]. CNT-TFTs are promising for flexible electronics because of their high mobility, substrate-neutrality, low-temperature fabrication process, etc [12,13]. As sensor material, CNTs have large surface area and exhibit charge-sensitive conductance, which attributes to the carbon atoms and C—C bonds on the tube surface [14]. The conductance of CNTs are known to be sensitive to ambient environment, especially to oxygen and oxygen-containing gaseous species [15,16]. In addition, CNT sensors can also work for the detection of hydrogen (H_2) [17,18], organic vapors [19], alcohols [20], etc. which has huge practical significance for disease and health diagnosis [21–23]. CNT sensors can also benefit from their low cost, room temperature operation, nanoscale and microelectronics applications [10,11,24].

The first CNT gas sensor was reported in 2000 by Kong et al. [25]. Since then, multiple studies have been performed to investigate the sensing behavior of CNT based devices. Reports on the sensing mechanism have been discussed and argued till today. Early discussions mainly focused on the adsorption of gas molecules at the CNT junction area [26], indirect interaction through pre-adsorbed water layer or the hydroxyl group from SiO_2 substrate [27], direct charge transfer between gas molecules and CNTs [28], and Schottky barrier modulation at the CNT/metal contacts [14], etc. Battie et al. performed experiments based on the CNT network and suggested gas molecules mainly attach to the CNT network, not CNT/metal contacts [29]. Later, Boyd et al. pointed out that the gas sensitivity is due to both the CNT/metal contacts and the CNT junctions, and the network effects are dominated by gas-induced changes in the CNT junctions [30]. As for sensitivity, a detection limit of 3 ppb ammonia (NH_3) was demonstrated by Rigoni et al [3].

Functionalization strategies, including polymers coating [31] or CNT decoration with different metal nanoparticles [32,33], were performed and yielded promising results for gas sensing. Kuzmych et al. functionalized the SWCNT networks with poly-(ether imide) noncovalently to detect NO in exhaled breath, leading to detection limit as low as 5 ppb in air [34]. Guerin et al. fabricated different electrode metals on top of horizontal CNT arrays [35]. These structures can take advantage of the specific interaction for each metal/CNT/gas case to discriminate different gas types. Abdelhalim et al. utilized different

* Corresponding author.
E-mail addresses: jlchen@gatech.edu, cjlsjtu@gmail.com (J. Chen).

https://doi.org/10.1016/j.snb.2018.10.035
Received 1 March 2018; Received in revised form 17 September 2018; Accepted 6 October 2018
Available online 10 October 2018
0925-4005/

metals to alter the response of each sensing element towards different sensing gases, which is capable of discriminating between four gases: NH_3, CO, CO_2, and ethanol [33]. But these methods degraded the overall performance of the sensors in terms of response rate and long term stability. Random CNT network and aligned CNT network in sensors were also investigated with single decorated molecules and nanoparticles [36,37], either in chambers [38] or in air [3]. However, only few researches focused on the selectivity of CNT sensors, and no publication has been reported on gas identification study without functionalization or coating.

In this work, CNT-TFTs as gas sensors were fabricated using randomly distributed CNT network. Sensor response from NH_3 and nitrogen dioxide (NO_2) spray at 2 ppm–40 ppm were measured in air at room temperature. The convolution based model was found to be a perfect match to the response curves. For a given CNT-TFT, the time constants of double exponential function were surprisingly independent of gas concentration while vary with respect to different gas types. More importantly, this uniqueness in time constants can be considered as its inherent identity with respect to different sensing gases, which can be used for gas identity verification. The verification process is proved to be very reliable when using single TFT, which is ultimately rooted in the randomness of CNT network. The verification can be applied to other gases such as H_2 and its accuracy can be further guaranteed when using multiple TFTs in parallel.

2. Experimental methods

2.1. Device fabrication and I–V measurement

CNT-TFTs were fabricated at the Institute for Electronics and Nanotechnology (IEN) cleanroom of Georgia Tech. Photolithography and lift-off process were performed to pattern gate (G), source/drain (S/D), and channel area. Fabrication flow chart is depicted in Fig. 1. To be specific, Ti/Au layers as back gate were deposited on top of a Si wafer by e-beam evaporation with deposition rate of 0.2 Å/s and 1 Å/s, respectively. Then atomic layer deposition (ALD) was used to deposit TiO_2 and HfO_2, covering the entire wafer surface as a global gate-dielectric layer. Both Ti and TiO_2 work as adhesion layers for gate and gate dielectric. 15 ~ 30 s oxygen plasma treatment was crucial to make the surface hydrophilic, followed by CNT network deposition by immersing the wafer into 0.01 ~ 0.02 g/L toluene-based CNT solution for 5–20 minutes (CNT source: > 99% purity polymer-wrapped CNT solution from NanoIntegris). After that, Ti/Au patterns were defined as S/D electrodes, followed by another photolithography for PR pattern and then 30 s oxygen plasma treatment to form channel area. At last, vacuum annealing at 250 °C for 2 h was performed to get rid of surface residue. The final features and CNT network are exhibited in Fig. 2(a).

The I–V characteristics of the CNT-TFTs had been measured using Microtech Summit 11k probe station and Keithley 4200-SCS. We fabricated series of devices with different channel lengths (L) and different channel widths (W). The output characteristics (I_d-V_{ds} curves) of the CNT-TFTs is shown in Fig. 2(b) for different channel lengths (L = 20 μm, 40 μm, 60 μm, and 100 μm) with V_{ds} swept from 0 to −2 V at V_{gs} = −1 V. For the transfer characteristics (I_d-V_{gs} curves), V_{gs} was swept from −2 to 2 V while keeping V_{ds} = −1 V. Semi-log plots are shown in Fig. 2(c) for each channel length. The overall I–V characteristics shows good performance of p-type CNT-TFTs with on/off ratio as high as 10^{-5} and mobility around 5 .

2.2. Experiment setup

The experiment setup for CNT-TFT based gas sensing measurement is depicted in Fig. 3. Gas spray was applied directly to the channel area of a TFT with Keithley 2604B source measurement units (SMUs) recording the current change over time. The nozzle, with inner diameter of 5 mm, was large enough to generate stable gas flow to cover the entire surface of the target TFT (0.25 mm × 0.75 mm). Only one TFT was tested each time. The applied gas was nitrogen (N_2, gas tank 1) mixed with either NH_3 (gas tank 2) or NO_2 (gas tank 2) at different ppm concentrate level (2 ppm, 10 ppm, 20 ppm, 40 ppm, etc.) controlled by ALICAT flowmeters. The CCD camera helped probe the target TFT before sensing. The whole setup was located inside fume hood under atmosphere pressure and stable room temperature.

During measurement, the target TFT was biased with V_{ds} = −0.5 V and V_{gs} = −1 V. We first apply this bias to the TFT for more than 20 min in order to stabilize the drain current (I_d). When I_d went smoothly, open the valves to release the gas mixture (either N_2 + NH_3 or N_2 + NO_2) while keep the mass flowrate constant at 1000 sccm all the time. After 10 min of gas spray (gas on state), we close the valves (gas off state) and keep the gas off state for 20 ~ 30 min before another sensing cycle began at a higher ppm level. The lowest concentrate we used was 2 ppm for both NH_3 and NO_2 sensing, which is higher enough to get rid of the possible noise effect since the CNT-TFTs might also detect interfering gases (such as NH_3, NO_2, H_2, etc.) at ppb level from the environment.

3. Results and discussion

3.1. Sample characteristics and the sensing mechanism

The sensor response under 2-cycle (2 ppm and 40 ppm) of NH_3 or NO_2 pulsing is shown in Fig. 4 for a long-channel CNT-TFT with L = 80 μm/W = 100 μm (2 K) and a short-channel CNT-TFT with L = 8 μm/W = 100 μm (2 H). They all show stable sensor response to

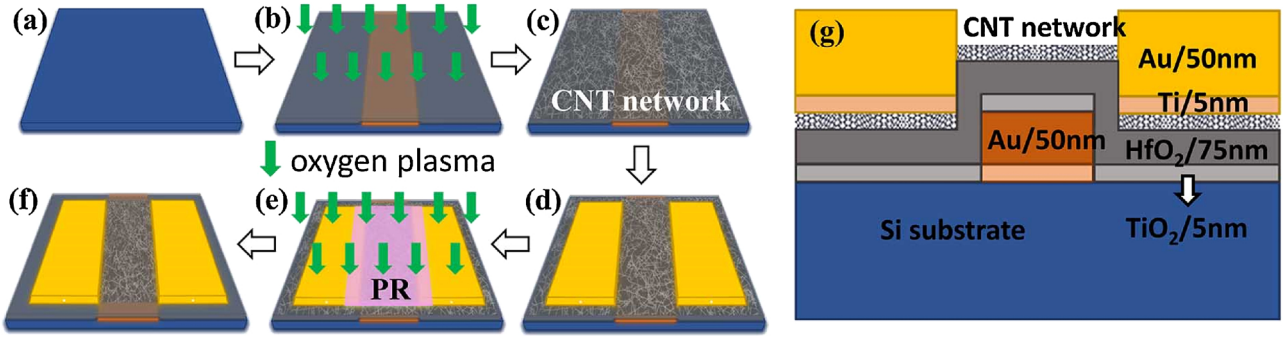

Fig. 1. Fabrication of CNT-TFTs. (a) Clean Si wafer washed by acetone, IPA, and DI water respectively. (b) Gate pattern and gate dielectric deposition, followed by oxygen plasma (green arrows) treatment to make the surface hydrophilic. (c) CNT network growth using toluene-based high purity CNT solution. (d) S/D electrodes pattern. (e) Photoresist (PR) thin layer as shield to protect CNT network in channel area, followed by oxygen plasma to etch away unwanted CNT network. (f) The CNT-TFT after PR dissolved by acetone. (g) The sectional view of the CNT-TFT (For interpretation of the references to colour in this figure legend, the reader is referred to the web version of this article).

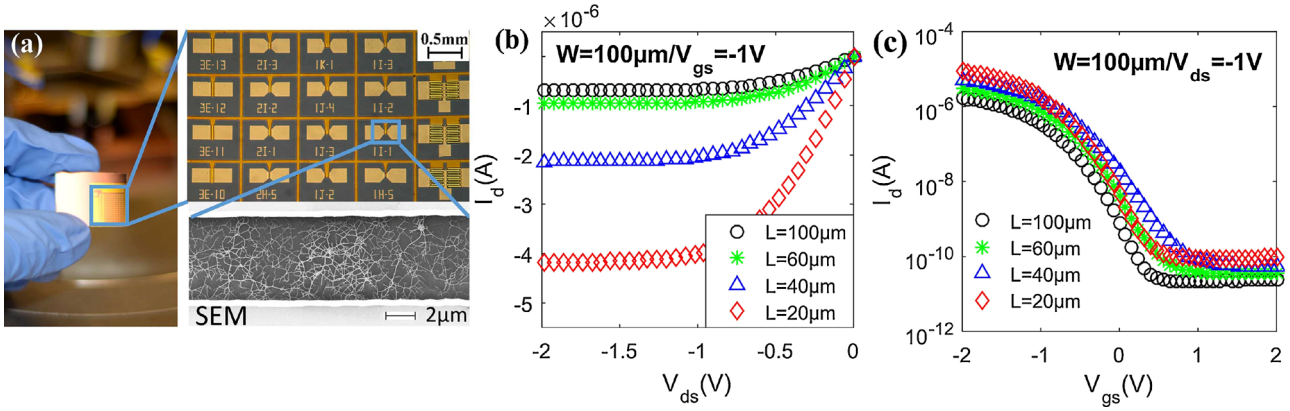

Fig. 2. Fabricated CNT-TFTs and corresponding I–V characteristics. (a) CNT-TFTs layout and the scanning electron microscope (SEM) image of CNT network. (b) Output characteristics of TFTs for various channel lengths and the same channel width. (c) Transfer characteristics of the same TFTs as in (b).

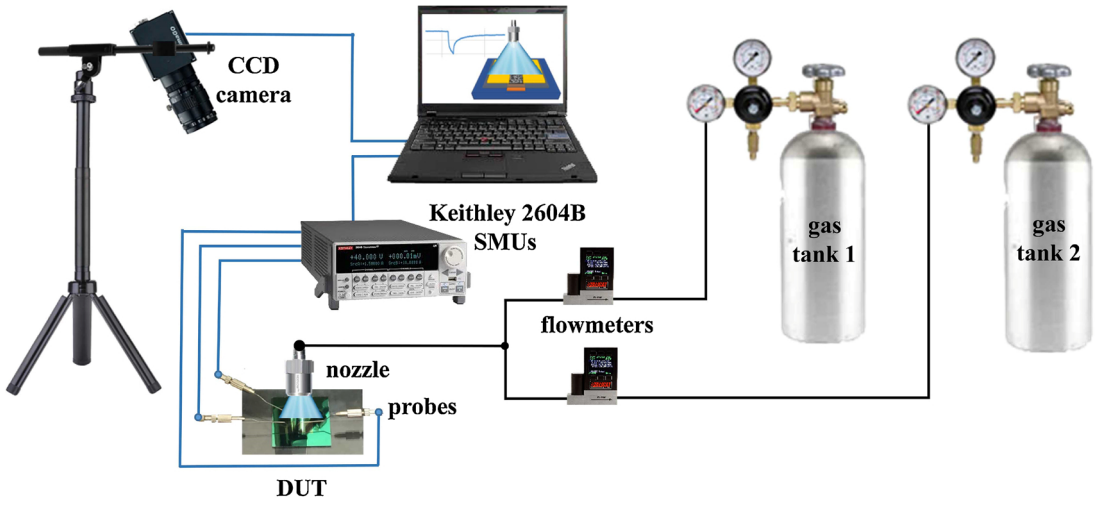

Fig. 3. Schematic diagram of the experiment setup for gas sensing.

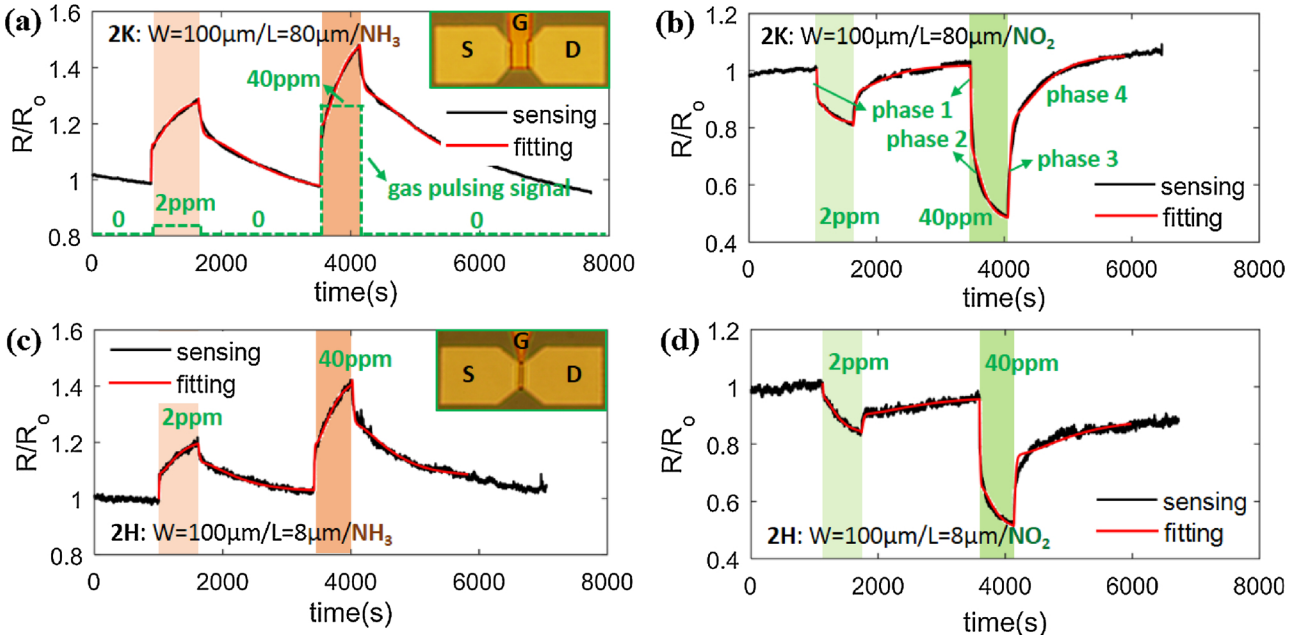

Fig. 4. 2-cycle (2 ppm and 40 ppm) sensor response under NH_3 or NO_2 spray for a long channel TFT (2 K: W = 100 μm/L = 80 μm) and a short-channel TFT (2H: W = 100 μm/L = 8 μm). R_o is the stable device resistance before gas spray. (a)-(b) Sensor response of 2 K under NH_3 or NO_2 spray respectively. (c)-(d) Sensor response of 2H under NH_3 or NO_2 spray respectively. Inset figures are the corresponding TFTs. Red curves are the fitting results using common time constants of double exponential-convolution model (For interpretation of the references to colour in this figure legend, the reader is referred to the web version of this article).

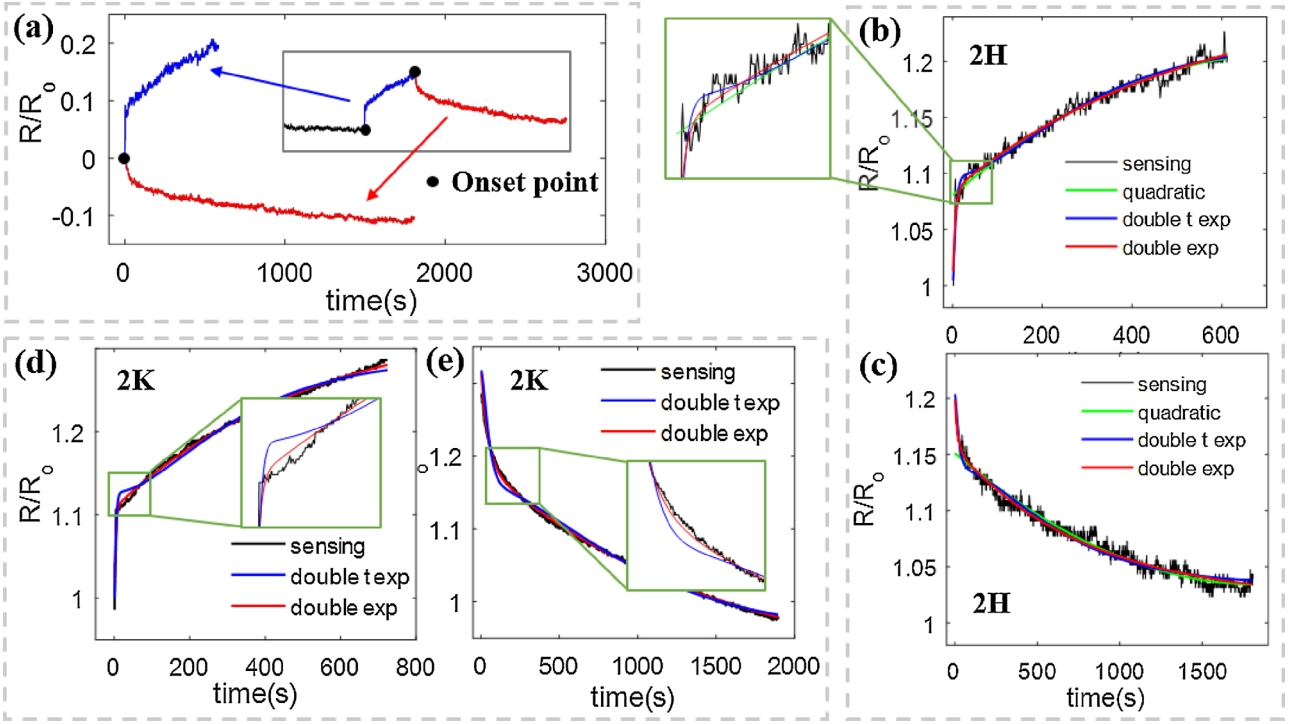

Fig. 5. Fitting for sensor response curves. (a) Linear transformation before fitting to standardize the fitting process for different sensing gas. (b)-(c) Fitting result comparison of device 2H in gas on and off state between double exponential-convolution (double exp) model, double t exponential-convolution (double t exp) model, and quadratic model. (d)-(e) Fitting result comparison of device 2 K in gas on and off state between double exponential and double t exponential models.

either NH_3 or NO_2 sensing. For each gas sensing process, the gas pulsing signal stayed for 10 min in 'on state' (shown as orange stripes for NH_3 or green stripes for NO_2 in figures) and 30 min in 'off state' (no stripe in figures) between each cycle. When NH_3 molecules interact with the CNT network in the channel area, they work as electron source which decreases the current by consuming the holes in the channel of the p-type CNT-TFT. Thus the resistance will increase during on state and decrease during off state. NO_2 affects the resistance in an opposite way by providing more holes to the channel. For 2 ppm concentration, both TFTs have more than 20% increase or decrease in resistance when exposed to NH_3 and NO_2. While for 40 ppm concentration, both TFTs show more than 50% resistance decrease under NO_2 spray and more than 40% resistance increase under NH_3 spray.

From the sensor response curves, it is easy to find 4 phases within each gas spray cycle, described in Fig. 4(b) in bold green, which is vital to understand the sensing mechanism for CNT-TFT based sensors. We define the interactive units between gas molecules and the device as dwelling spots, which largely exist in CNT-CNT junctions, CNT-metal area, and other locations such as defects on CNTs. A dwelling spot can either capture or release a gas molecule depending on it is taken already or not. For a gas spray cycle, phase 1 is the beginning of gas on state, where the resistance experiences an abrupt change when large number of empty dwelling spots are being taken by the gas molecules. Phase 1 only lasts for several seconds when all gas molecules can unlimitedly take the empty spots, which counts for a significant proportion of the resistance change during the entire on state. Even though gas molecules can escape their dwelling spots all the time, it can be ignored compared to the amount of gas molecules that take the empty spots. Phase 2 starts when a large number of the empty spots have already been taken. In this phase, endless gas molecules reach the channel surface continuously like phase 1, but only part of them can be taken by the dwelling spots because some of them will reach unavailable spots, which slows down the rate of change in resistance compared to phase 1. Another cause is, more and more trapped molecules can escape their spots than phase 1. Even after saturation, the target TFT is in a dynamic equilibrium with the escaping molecules cancelling out the molecules being taken by the dwelling spots. Phase 3 begins when gas spray comes to an end and no molecule reaches the channel surface (gas off state). Conversely, there are a large number of gas molecules escaping their spots, resulting in the abrupt change in resistance which is similar to phase 1 but in an opposite manner. In phase 4, the change rate slows down because it is more difficult for the remaining trapped molecules to escape their spots. Physically, it is well known that the dwelling spots near CNT junctions and CNT-metal region are much easier to capture gas molecules (gas molecules are relatively stable and harder to escape in those spots) than CNT itself and other region of the channel. Therefore, the slowness in phase 4 mainly results from the difficulty of gas molecules escaping from CNT junctions and CNT-metal region, while the sudden change in resistance of phase 3 mainly attributes to the rapid escape of gas molecules from CNT itself and other similar unstable gas-dwelling spots.

3.2. Sensor response fitting

Enlightened by the two phases during gas on or gas off state, it is natural to resort to double exponential function for fitting purpose. There are two formats related to double exponential function

$$f_1(t) = a\cdot\exp(-t/\tau_a) + b\cdot\exp(-t/\tau_b) \quad (1)$$

$$f_2(t) = a\cdot t\cdot\exp(-t/\tau_a) + b\cdot t\cdot\exp(-t/\tau_b) \quad (2)$$

where τ_a and τ_b are time constants, t is time, a and b are constants. To distinguish these two formats, we define Eq. (1) as double exponential function, Eq. (2) as double t exponential function. The gas pulsing signal can be expressed as

$$g(t) = \begin{cases} h & gas\ on \\ 0 & gas\ off \end{cases} \quad (3)$$

where the constant h is the height of the pulse signal.

Rigoni et al. once used convolution between double t exponential

function and gas pulsing signal to fit the sensor response curves of a whole cycle using the same time constants [3]. However, we found convolution between double exponential function and gas pulsing signal is a better match for sensor response curves. To be specific, let *D(t)* be the original sensor response data, e.g., the sensor response curves in Fig. 4. To fit *D(t)* separately for gas on state and gas off state in each case, linear transformation was applied to move both gas on state and gas off state to the origin from the onset point, exhibited in Fig. 5(a). Obviously linear actions will not change the time constants. Then we resorted to double exponential-convolution model to fit the sensor response curves separately. That is

$$D_{f1}(t) = f_1(t) \otimes g(t) \tag{4}$$

where $D_{f1}(t)$ is the fitting results from convolution between double exponential function and gas pulsing signal. We consider $a = 1$ to eliminate a redundant variable during fitting. Then apply linear transformation for $D_{f1}(t)$ in order to restore the real time fitting

$$D_f(t) = D_{f1}(t - t_o) + D(t_o) \tag{5}$$

Where *D(t)* is the original sensor response data, t_o is the time at the onset point. The standard deviation

$$\sigma = ||D_f(t) - D(t)|| = \sqrt{\frac{1}{N}\sum_{i=1}^{N}(D_f(t_i) - D(t_i))^2} \tag{6}$$

is defined for error evaluation. Same process is applied for double t exponential-convolution model by using *f2* instead of *f1*.

Fig. 5(b)–(c) compares the fitting results of 2H between double exponential-convolution model, double t exponential-convolution model, and quadratic model. From the fitting curves, double exponential-convolution model matches the original sensor response data the best in both states. It is quite clear that the quadratic model is unable to depict the sudden change at the beginning of the each state (phase 1 and phase 3). While for double t exponential-convolution model, the fitting is distorted during the transition period between each phase. Quantitatively, the standard deviations (σ) for double exponential-convolution model, double t exponential-convolution model, and quadratic model during gas on state are 3.65×10^{-5}, 4.24×10^{-5}, and 6.68×10^{-5} respectively. And for gas off state, the corresponding standard deviations are 3.15×10^{-5}, 4.31×10^{-5}, and 4.55×10^{-5}. Therefore, double exponential-convolution model can best fit the sensor response curves. Fig. 5(d)–(e) further confirm the superior of double exponential-convolution model. Other fitting cases also support the same conclusion.

3.3. Consistency of time constants for different concentration

During sensor response fitting from double exponential-convolution model, we noticed the two time constants (τ_a and τ_b) in Eq. (1) are quite stable for sensing at different gas concentrations. Based on that observation, we assumed the same τ_a and τ_b (common time constants) while fitting response of the same TFT during gas sensing at different concentrations. The fitting results are shown in Fig. 4. The common time constants and the corresponding fitting errors are listed in Table 1. Surprisingly, the fitting are excellent for both NH_3 and NO_2 spray in either gas on state or gas off state. Fig. 6 shows the fitting results for another TFT at 4 different gas concentrations, which are 2 ppm, 10 ppm, 20 ppm, and 40 ppm. The excellence in sensor response fitting from both Figs. 4 and 6 demonstrates the consistency of the common time constants with respect to different gas concentration.

4-cycle gas sensing of NO_2 spray were performed with different flowrates (600 sccm, 800 sccm, 1000sccm, and 1200sccm) but at the same concentration of 50 ppm. This 4-cycle gas sensing is used to analyze the impact of nozzle pressure, which is a function of the flowrate. The sensor response and corresponding fitting results are plotted in Fig. 7. It is easy to observe that the nozzle pressure has significant impact on sensitivity, i.e., the resistance (R/R_o) increases with increasing flowrate/pressure. The corresponding values of R/R_o are 0.83 (600 sccm), 0.62 (800 sccm), 0.55 (1000sccm), and 0.52 (1200sccm). However, the sensor responses can still be well described with low fitting errors by common time constants obtained from the double exponential-convolution model in this 4-cycle sensing test, which is similar to time constants used in Fig. 6. Therefore, the two time constants, which mainly depend on the device morphology (CNT network structure, CNT-metal contacts, etc.), are very stable under the change of nozzle pressure.

Table 1
Common time constants at different gas concentration in each state and the corresponding fitting errors.

Device	State	(τ_a, τ_b)	σ
2K	NH_3 on	(471, 5.0)	3.22×10^{-5}
	NH_3 off	(1879, 38.6)	1.88×10^{-5}
	NO_2 on	(227, 10.9)	12.2×10^{-5}
	NO_2 off	(843, 51.0)	6.37×10^{-5}
2H	NH_3 on	(514, 5.7)	3.85×10^{-5}
	NH_3 off	(801, 17.3)	4.85×10^{-5}
	NO_2 on	(328, 10.3)	8.26×10^{-5}
	NO_2 off	(1723, 30.3)	15.9×10^{-5}

3.4. Gas identity verification

For a given CNT-TFT, the two time constants, (τ_a, τ_b) pair, are unique for either gas on state or gas off state and do not depend on the gas concentration. More importantly, (τ_a, τ_b) pair changes with respect to different gas types. Therefore, the one-to-one mapping between time constants and gas types can be regarded as the inherent properties for a given TFT, which can be used for gas identity verification depending on the corresponding error difference. Take the device 2 K in Fig. 4(a) as an example, (τ_a, τ_b) pair for different gas sensing in different states can be determined easily from tentative testing for calibration purpose, shown in Table 1. For an unknown sensing gas (e.g., either NH_3 or NO_2), let 2 K record the sensor response for a cycle. Based on (τ_a, τ_b) pairs from different assumptions, the corresponding fitting errors can be obtained, shown in Fig. 8. It is clear that (τ_a, τ_b) = (471, 5.0) from NH_3 assumption can perfectly fit the sensor response curve while the fitting is distorted when (τ_a, τ_b) = (227, 10.9) from NO_2 assumption. Quantitatively, the fitting error is $\sigma = 3.22 \times 10^{-5}$ when (τ_a, τ_b) = (471, 5.0) during gas on state, while $\sigma = 17.57 \times 10^{-5}$ when (τ_a, τ_b) = (227, 10.9). That means the fitting error from NO_2 assumption is more than 5 times larger than NH_3 assumption. Therefore we can safely conclude the unknown gas is NH_3, not NO_2. Same conclusion can be drawn from the corresponding error difference during gas off state, shown in Fig. 8. Without any doubt, this is actually a general strategy that can be easily applied for identity verification for more gases. This gas identification strategy is proved to be valid for gas sensing with different flowrates (different nozzle pressure), which is confirmed by conducting sensing test with different flowrates ranging from 600 sccm to 1200sccm.

The cycling experiment has been conducted under NO_2 spray at the same concentration considering possible external influence (e.g., humidity, other possible sensing noise) during sensing test at different time. The corresponding sensor responses are plotted in Fig. 9 at 5 h' time difference. During this period, the target sensor is put in air in order to ensure the full interaction with surrounding environment for enough time. Fitting 1 is based on common time constants and fitting 2 is based on separate time constants (performed separately for each cycle, which is the best fitting from the convolution model). As shown in Fig. 9, the overall errors from fitting 2 are 2.26×10^{-5} and 6.94×10^{-5} in gas on and gas off state respectively. As for fitting 1, those values are 3.11×10^{-5} and 9.22×10^{-5}, which means the changes are acceptable between fitting 1 and fitting 2. However, the error difference between

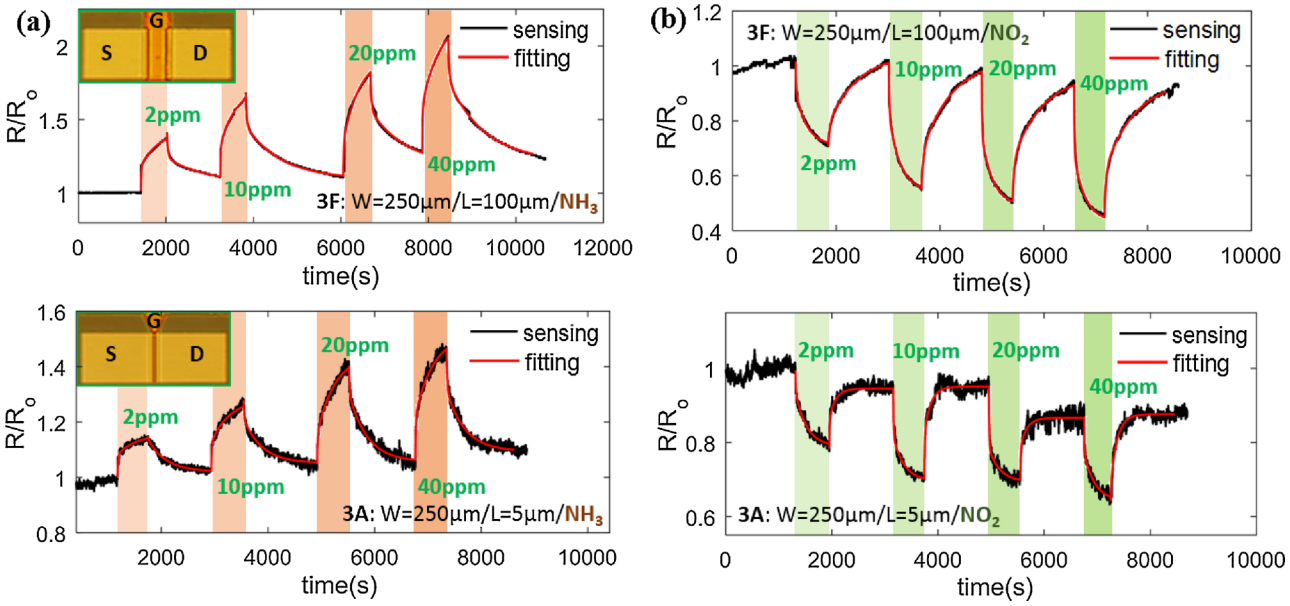

Fig. 6. 4-cycle (2 ppm, 10 ppm, 20 ppm, 40 ppm) sensor response and the corresponding fitting, using common time constants of double exponential-convolution model at different gas concentration. (a)–(b) Results for a long channel device 3 F. (c)-(d) Results for a short channel device 3 A.

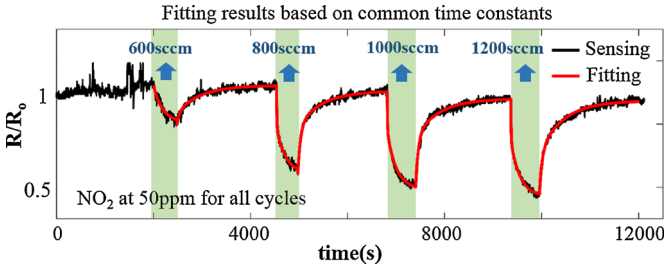

Fig. 7. 4-cycle sensor response under NO_2 spray and the corresponding fitting using common time constants of double exponential-convolution model with different flowrates (600 sccm, 800 sccm, 1000sccm, 1200sccm) but at the same concentration of 50 ppm.

different gas assumptions (NH_3 and NO_2) is as large as 10 times (1000%) for gas identification. Therefore, the external influence is very limited, which will not affect the accuracy of gas identification.

Theoretically, this identification process can be conducted through only one state from a single sensing cycle because of the uniqueness of (τ_a, τ_b) pair. Fig. 10 maps the (τ_a, τ_b) pairs for more TFTs under NH_3 and NO_2 spray. The scattered marks reveal the uniqueness of (τ_a, τ_b) pair with respect to different gas types for different TFTs. On the one hand, for a given TFT, there is no overlapped or even close (τ_a, τ_b) pairs with respect to different gases. On the other hand, for a given sensing gas, there is no overlapped or even close (τ_a, τ_b) pairs with respect to different TFTs either. This uniqueness mainly roots in the randomness of CNT network inside the channel area, which is different with respect to CNT network density, CNT network structure, and channel dimensions, etc.

However, in practice, some (τ_a, τ_b) pairs might be very close to each other and cause interference when considering sensing cases for more possible gases. Many causes contribute to this such as ambience noise, unstable gas spray, experimental errors, etc. To address this problem, more tentative testing for a better calibration is vital in order to obtain the authentic time constant pairs for each gas sensing case. Similarly,

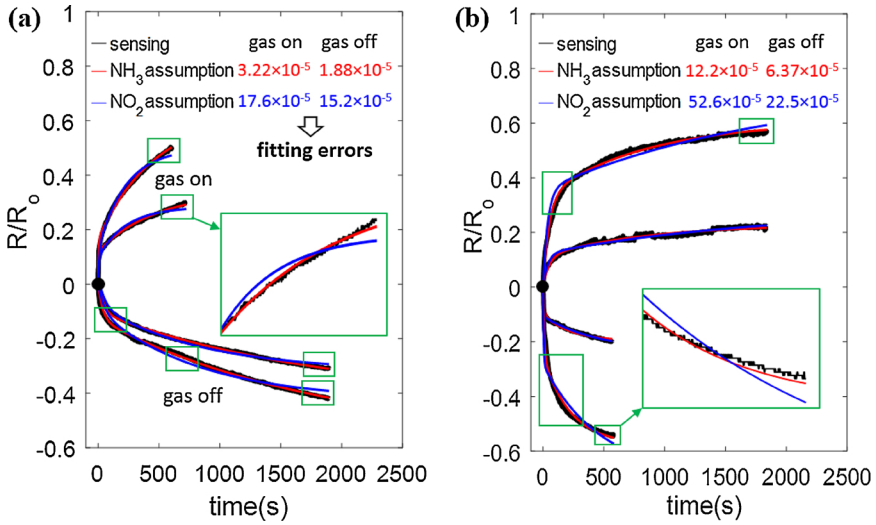

Fig. 8. Gas identification based on the common time constant and the corresponding error difference. (a) Fitting results from different gas assumptions (time constant pairs) for device 2 K in gas on state. (b) Same strategy as (a) for device 2 K in gas off state.

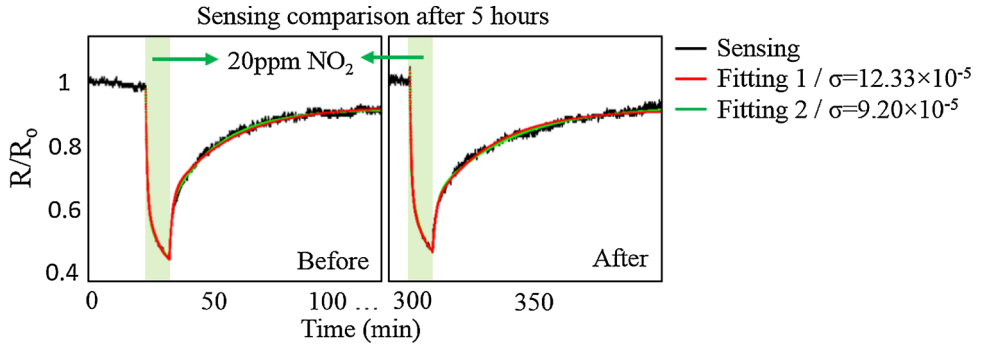

Fig. 9. The cycling sensing experiment and comparison of the corresponding sensor responses under NO_2 spray at the same concentration (20 ppm) for the same device at 5 h' time period. Fitting 1 is based on common time constants and fitting 2 is based on separate time constants.

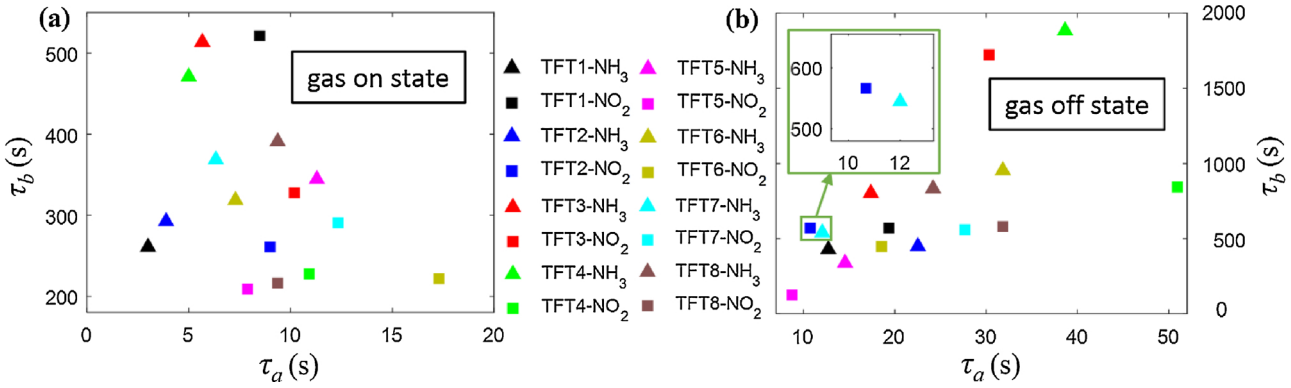

Fig. 10. One-to-one mapping for time constant pairs (τ_a, τ_b) in gas on state (a) and gas off state (b). The same marks denote the same gas type, and the same colors represent the same device.

performing multiple sensing cycles are also crucial during identity verification process. More efficiently, different TFTs can be used in parallel for gas identification instead of using just one, which helps avoid the possibility that the difference in fitting errors might be on the same level. Generally, the smoother sensor response from longer channel TFTs are more reliable for gas identification because of the larger difference in fitting errors. From most cases we experienced, one TFT is enough for the verification process.

4. Conclusion

CNT-TFT based gas sensors have been fabricated with randomly distributed CNT network and sensor response under NH_3 and NO_2 spray at low ppm level have been tested. The different phases for gas response within each cycle suggest the sensing mechanism is based on the interaction between gas molecules and different types of dwelling spots inside the device. We develop double exponential-convolution model to fit the sensor response. The two time constants of double exponential function are found to be independent of gas concentration, but vary with respect to different gas types and different TFTs. This can be used for gas identification because of the uniqueness of the time constants for different gas types. We ascribe this uniqueness to the randomness of CNT network in channel area, which help build a unique channel structure for each TFT and thus create the diversity in dwelling spots for gas molecules during sensing process. By comparing the large difference in fitting errors, this one-to-one dependence between time constants and the sensing gases is successfully used for gas identity verification between NH_3 and NO_2. More significantly, it actually provides a general and practical strategy for identity verification over more gases without distinction. In perspective, this analysis manages to create the selectivity of SWCNT based sensors with respect to different gases, which will largely broaden their applications in practice.

References

[1] M. Meyyappan, Carbon nanotube-based chemical sensors, Small 12 (16) (2016) 2118–2129.
[2] D. Kumar, P. Chaturvedi, P. Saho, P. Jha, A. Chouksey, M. Lal, J. Rawat, R. Tandon, P. Chaudhury, Effect of single wall carbon nanotube networks on gas sensor response and detection limit, Sens. Actuators, B 240 (2017) 1134–1140.
[3] F. Rigoni, S. Tognolini, P. Borghetti, G. Drera, S. Pagliara, A. Goldoni, L. Sangaletti, Enhancing the sensitivity of chemiresistor gas sensors based on pristine carbon nanotubes to detect low-ppb ammonia concentrations in the environment, Analyst 138 (24) (2013) 7392–7399.
[4] L. Xue, W. Wang, Y. Guo, G. Liu, P. Wan, Flexible polyaniline/carbon nanotube nanocomposite film-based electronic gas sensors, Sens. Actuators, B 244 (2017) 47–53.
[5] K. Lee, V. Scardaci, H.-Y. Kim, T. Hallam, H. Nolan, B.E. Bolf, G.S. Maltbie, J.E. Abbott, G.S. Duesberg, Highly sensitive, transparent, and flexible gas sensors based on gold nanoparticle decorated carbon nanotubes, Sens. Actuators, B 188 (2013) 571–575.
[6] S. Nag, A. Sachan, M. Castro, V. Choudhary, J. Feller, Spray layer-by-layer assembly of POSS functionalized CNT quantum chemo-resistive sensors with tuneable selectivity and ppm resolution to VOC biomarkers, Sens. Actuators, B 222 (2016) 362–373.
[7] J. Li, L. Hu, J. Liu, L. Wang, T.J. Marks, G. Grüner, Indium tin oxide modified transparent nanotube thin films as effective anodes for flexible organic light-emitting diodes, Appl. Phys. Lett. 93 (8) (2008) 310.
[8] B. Kim, S. Jang, M.L. Geier, P.L. Prabhumirashi, M.C. Hersam, A. Dodabalapur, High-speed, inkjet-printed carbon nanotube/zinc tin oxide hybrid complementary ring oscillators, Nano Lett. 14 (6) (2014) 3683–3687.
[9] C.M. Homenick, R. James, G.P. Lopinski, J. Dunford, J. Sun, H. Park, Y. Jung, G. Cho, P.R. Malenfant, Fully printed and encapsulated SWCNT-based thin film transistors via a combination of R2R gravure and inkjet printing, ACS Appl. Mater. Interfaces 8 (41) (2016) 27900–27910.
[10] K. Chen, W. Gao, S. Emaminejad, D. Kiriya, H. Ota, H.Y.Y. Nyein, K. Takei, A. Javey, Printed carbon nanotube electronics and sensor systems, Adv. Mater. 28 (22) (2016)

4397–4414.
[11] Y. Cao, S. Cong, X. Cao, F. Wu, Q. Liu, M.R. Amer, C. Zhou, Review of electronics based on single-walled carbon nanotubes, Top. Curr. Chem. 375 (5) (2017) 75.
[12] E. Artukovic, M. Kaempgen, D. Hecht, S. Roth, G. Grüner, Transparent and flexible carbon nanotube transistors, Nano Lett. 5 (4) (2005) 757–760.
[13] J. Chen, S. Kumar, Variability in output characteristics of single-walled carbon nanotube thin-film transistors, IEEE Trans. Nanotechnol. 17 (2) (2018) 353–361.
[14] N. Peng, Q. Zhang, C.L. Chow, O.K. Tan, N. Marzari, Sensing mechanisms for carbon nanotube based NH3 gas detection, Nano Lett. 9 (4) (2009) 1626–1630.
[15] Y. Wang, K. Zhang, J. Zou, X. Wang, L. Sun, T. Wang, Q. Zhang, Functionalized horizontally aligned CNT array and random CNT network for CO 2 sensing, Carbon 117 (2017) 263–270.
[16] T. Zhang, S. Mubeen, N.V. Myung, M.A. Deshusses, Recent progress in carbon nanotube-based gas sensors, Nanotechnology 19 (33) (2008) 332001.
[17] A.A. Abdelwahab, Electrochemical pretreatment of graphene composite CNT encapsulated Au nanoparticles for H2O2 sensor, Electroanalysis 28 (8) (2016) 1901–1906.
[18] B. Sharma, H. Yadav, J.-S. Kim, MEMS based hydrogen sensor with the highly porous Au-CNT film as a sensing material, J. Mater. Sci.: Mater. Electron. (2017) 1–8.
[19] S. Badhulika, N.V. Myung, A. Mulchandani, Conducting polymer coated single-walled carbon nanotube gas sensors for the detection of volatile organic compounds, Talanta 123 (2014) 109–114.
[20] C.B. Jacobs, M.J. Peairs, B.J. Venton, Carbon nanotube based electrochemical sensors for biomolecules, Anal. Chim. Acta 662 (2) (2010) 105–127.
[21] Y. Adiguzel, H. Kulah, Breath sensors for lung cancer diagnosis, Biosens. Bioelectron. 65 (2015) 121–138.
[22] B. Kim, Y. Lu, T. Kim, J.-W. Han, M. Meyyappan, J. Li, Carbon nanotube coated paper sensor for damage diagnosis, ACS Nano 8 (12) (2014) 12092–12097.
[23] F.R. Baptista, S. Belhout, S. Giordani, S. Quinn, Recent developments in carbon nanomaterial sensors, Chem. Soc. Rev. 44 (13) (2015) 4433–4453.
[24] B. Chen, P. Zhang, L. Ding, J. Han, S. Qiu, Q. Li, Z. Zhang, L.-M. Peng, Highly uniform carbon nanotube field-effect transistors and medium scale integrated circuits, Nano Lett. 16 (8) (2016) 5120–5128.
[25] J. Kong, N.R. Franklin, C. Zhou, M.G. Chapline, S. Peng, K. Cho, H. Dai, Nanotube molecular wires as chemical sensors, Science 287 (5453) (2000) 622–625.
[26] J. Zhao, A. Buldum, J. Han, J.P. Lu, Gas molecule adsorption in carbon nanotubes and nanotube bundles, Nanotechnology 13 (2) (2002) 195.
[27] T. Someya, J. Small, P. Kim, C. Nuckolls, J.T. Yardley, Alcohol vapor sensors based on single-walled carbon nanotube field effect transistors, Nano Lett. 3 (7) (2003) 877–881.
[28] H. Chang, J.D. Lee, S.M. Lee, Y.H. Lee, Adsorption of NH 3 and NO 2 molecules on carbon nanotubes, Appl. Phys. Lett. 79 (23) (2001) 3863–3865.
[29] Y. Battie, O. Ducloux, P. Thobois, N. Dorval, J.S. Lauret, B. Attal-Trétout, A. Loiseau, Gas sensors based on thick films of semi-conducting single walled carbon nanotubes, Carbon 49 (11) (2011) 3544–3552.
[30] A. Boyd, I. Dube, G. Fedorov, M. Paranjape, P. Barbara, Gas sensing mechanism of carbon nanotubes: from single tubes to high-density networks, Carbon 69 (2014) 417–423.
[31] T. Zhang, S. Mubeen, E. Bekyarova, B.Y. Yoo, R.C. Haddon, N.V. Myung, M.A. Deshusses, Poly (m-aminobenzene sulfonic acid) functionalized single-walled carbon nanotubes based gas sensor, Nanotechnology 18 (16) (2007) 165504.
[32] A. Star, V. Joshi, S. Skarupo, D. Thomas, J.-C.P. Gabriel, Gas sensor array based on metal-decorated carbon nanotubes, J. Phys. Chem. B 110 (42) (2006) 21014–21020.
[33] A. Abdelhalim, M. Winkler, F. Loghin, C. Zeiser, P. Lugli, A. Abdellah, Highly sensitive and selective carbon nanotube-based gas sensor arrays functionalized with different metallic nanoparticles, Sens. Actuators, B 220 (2015) 1288–1296.
[34] O. Kuzmych, B.L. Allen, A. Star, Carbon nanotube sensors for exhaled breath components, Nanotechnology 18 (37) (2007) 375502.
[35] H. Guerin, H. Le Poche, R. Pohle, E. Buitrago, M.F.-B. Badía, J. Dijon, A.M. Ionescu, Carbon nanotube gas sensor array for multiplex analyte discrimination, Sens. Actuators, B 207 (2015) 833–842.
[36] E. Llobet, Gas sensors using carbon nanomaterials: a review, Sens. Actuators, B 179 (2013) 32–45.
[37] S. Li, J.G. Park, S. Wang, R. Liang, C. Zhang, B. Wang, Working mechanisms of strain sensors utilizing aligned carbon nanotube network and aerosol jet printed electrodes, Carbon 73 (2014) 303–309.
[38] P. Bondavalli, L. Gorintin, G. Feugnet, G. Lehoucq, D. Pribat, Selective gas detection using CNTFET arrays fabricated using air-brush technique, with different metal as electrodes, Sens. Actuators, B 202 (2014) 1290–1297.

Jialuo Chen received the B.S. degree from University of Shanghai for Science and Technology and the M.S. from Shanghai Jiao Tong University, Shanghai, China, in 2010 and 2013 respectively in mechanical engineering. Now he is currently pursuing the Ph.D. degree in electrical and computer engineering from Georgia Institute of Technology, Atlanta, GA, USA. His current research interests focus on Carbon nanotube network thin film transistors, including fabrication and their applications.

Ardalan Lotfi is a PhD student in mechanical engineering at Georgia Institute of Technology. His research interests include MEMS/NEMS sensor systems and Nanotechnology applications in environmental monitoring. He received his B.S. in Electrical Engineering from the University of Isfahan, Iran and a M.S. in Nanotechnology for ICT's from the Polytechnic of Turin, Italy.

Peter J. Hesketh received a B.Sc. from the University of Leeds (1979), and obtaining an M.S. (1983) Ph.D. (1987) in electrical engineering from the University of Pennsylvania. He is currently a Professor of mechanical engineering at Georgia Institute of Technology, Member of the Parker H. Petit Institute for Bioengineering and Biosciences, Member of the Institute for Electronics and Nanotechnology, and Director of the Micro and Nano Engineering Group in the School of mechanical engineering. His research interests include micro/nanofabrication techniques, MEMS based chemical gas sensors and gas chromatography systems, micro-magnetic actuators and microfluidics for sample preconcentration of microbial contamination. He has published over ninty journal papers and edited sixteen books on microsystems. He is a Fellow of the AAAS, ASME, ECS, a member of ASEE, Sigma Xi, and IEEE.

Satish Kumar received the Ph.D. degree in mechanical engineering and the M.S. degree in electrical and computer engineering from Purdue University, West Lafayette, IN, USA, in 2007. He is currently an associate professor at the George W. Woodruff School of mechanical engineering at Georgia Institute of Technology, Atlanta, GA, USA. He has authored or co-authored over 60 journal publications. Prof. Kumar is a recipient of the 2005 Purdue Research Foundation Fellowship, the 2012 Summer Faculty Fellowship from the Air Force Research Laboratories, the 2013 Woodruff School Teaching Fellowship, the 2014 DARPA Young Faculty Award, and the 2014 Sigma Xi Young Faculty Award.